JOM, Vol. 68, No. 7, 2016
DOI: 10.1007/s11837-016-1912-3

Quasi-Static and High Strain Rate Compressive Response of Injection-Molded Cenosphere/HDPE Syntactic Foam

B.R. BHARATH KUMAR,[1] ASHISH KUMAR SINGH,[2] MRITYUNJAY DODDAMANI,[1,3] DUNG D. LUONG,[2] and NIKHIL GUPTA[2,4]

1.—Lightweight Materials Laboratory, Department of Mechanical Engineering, National Institute of Technology - Karnataka, Surathkal, India. 2.—Composite Materials and Mechanics Laboratory, Mechanical and Aerospace Engineering Department, New York University Tandon School of Engineering, Brooklyn, NY 11201, USA. 3.—e-mail: mrdoddamani@nitk.edu.in. 4.—e-mail: ngupta@nyu.edu

High strain rate compressive properties of high-density polyethylene (HDPE) matrix syntactic foams containing cenosphere filler are investigated. Thermoplastic matrix syntactic foams have not been studied extensively for high strain rate deformation response despite interest in them for lightweight underwater vehicle structures and consumer products. Quasi-static compression tests are conducted at 10^{-4} s^{-1}, 10^{-3} s^{-1} and 10^{-2} s^{-1} strain rates. Further, a split-Hopkinson pressure bar is utilized for characterizing syntactic foams for high strain rate compression. The compressive strength of syntactic foams is higher than that of HDPE resin at the same strain rate. Yield strength shows an increasing trend with strain rate. The average yield strength values at high strain rates are almost twice the values obtained at 10^{-4} s^{-1} for HDPE resin and syntactic foams. Theoretical models are used to estimate the effectiveness of cenospheres in reinforcing syntactic foams.

INTRODUCTION

Particulate fillers are widely used in composite materials due to benefits such as low processing cost, high wear resistance, improvement in mechanical properties and high dimensional stability.[1] Reduction in cost plays a vital role in making these composites commercially viable. Use of industrial waste materials is increasing in such applications owing to the increasing thrust for finding new recycling avenues. Fly ash is an industrial waste material and is a by-product of coal combustion. Fly ash comprises ceramics that predominantly contain alumina and silica with small quantities of Fe_2O_3 and CaO.[2] A small percentage of fly ash particles are hollow, which are referred as cenospheres. These low-density cenospheres can be used in developing lightweight composite materials.

Hollow particles are dispersed in a matrix material to make lightweight composites known as syntactic foams.[3] These composites exhibit considerable densification of their porous microstructure under compressive loading and provide large failure strain.[4,5] Higher compressive modulus, strength, and energy absorption of syntactic foams make them promising materials in load-bearing structural applications. The moisture absorption characteristics of syntactic foams have been studied and this closed-cell foam structure has been found to be effective in keeping the overall moisture absorption low.[6,7] Structure–property correlations with constituent materials' geometrical parameters such as hollow particle wall thickness and volume fraction have been widely investigated in the literature, mainly for high quality engineered glass particles.[8–10] Development of newer syntactic foams for higher performance in aerospace, marine, and transportations applications[11,12] requires understanding high strain rate (HSR) responses of these materials.[13,14]

Strain rate sensitivity is an important issue in the transportation sector where crashworthiness is a major consideration. A large number of studies can be found in the literature on HSR characteristics of polymeric and metallic foams that are relevant to such applications.[15] These foams are intended to be used as fillers for A- and B-pillars, bumpers, and crumple zones, which are designed for impact and

(Published online April 11, 2016)

high strain rate loading conditions. Syntactic foams with higher energy absorption abilities can be candidate materials for similar applications. Dynamic tests have been conducted on a variety of rigid polymers using a drop weight tower or simulated head impact using a dynamic impact sled.[16] Mechanical properties of epoxy matrix syntactic foams are found to be strain rate sensitive.[13,17–19] These studies have observed that the strength of epoxy matrix syntactic foams increases with strain rate. Although the strain rate sensitivity can be primarily attributed to the matrix material,[20] the failure mechanism is affected by the wall thickness and volume fraction of hollow particles and their correlation needs detailed investigation.[21,22]

Thermoplastic resins have a higher level of viscoelasticity than thermosetting resins and are expected to have a stronger strain rate sensitivity in mechanical properties. Comprehensive studies relating the properties of various constituting materials to the HSR properties of thermoplastic syntactic foams are desired for developing materials tailored for the transportation sector. No studies are found in the literature to the best of the authors' knowledge on HSR compressive properties of high density polyethylene (HDPE) syntactic foams. The present work aims at filling this critical gap by (1) studying syntactic foams containing varying cenosphere content, (2) characterizing them over a wide range of compressive strain rates spanning seven orders of magnitude and (3) using theoretical models to understand the properties of cenospheres and evaluate their potential for use as fillers in composite materials. Cenospheres are the by-product ash of coal combustion in thermal power plants. These low-density hollow particles are made of ceramics such as alumina and silica. However, their structure contains defects and their properties are lower than those expected from engineered hollow particles of silica or alumina of the same true particle density. The experimentally validated theoretical models for syntactic foams can help in estimating the properties of cenospheres and provide insight into their potential for use as fillers in syntactic foams. Use of cenospheres as fillers can be beneficial as it can reduce the cost of syntactic foams and make them commercially viable in a number of applications, thus reducing landfill burden.

EXPERIMENTAL

Materials and Sample Preparation

HDPE of grade HD50MA180 (melt flow index of 20 g/10 min) procured from Reliance Polymers, Mumbai, India, was used as the matrix material. The HDPE resin was obtained in the form of granules of 3 mm diameter and has a mean molecular weight of 97,500 g/mol.

The cenospheres were of grade CIL-150 and supplied by Cenosphere, Kolkata, India. They are primarily made of SiO_2 (52–62%) and Al_2O_3 (32–36%) along with small quantities of other metal oxides as seen in Table I. Cenospheres were used in the as-received condition without any surface treatment.

A Quantachrome Ultrapyc 1000 pycnometer was used to measure the true particle density of cenospheres, which is 0.8517 g/cm^3. Particle size analysis was conducted using a Sympatec (Pennington, NJ) QICPIC high speed image analysis system. The measured average particle size was 76.33 ± 32 μm.

Syntactic foams were fabricated by mechanically pre-mixing HDPE and cenospheres in the desired proportion and loading the mixture into the hopper of a horizontal type plastic injection molding (PIM) machine (WINDSOR, 80 ton capacity). In the machine, a screw rotates at 30 rpm in the heating chamber dispersing cenospheres uniformly in the plasticized HDPE. The mixture is then injected through the nozzle into a mold of the desired dimensions. The operating parameters of the PIM machine for molding cenosphere/HDPE syntactic foam specimens were optimized in an earlier study[23] and set at a temperature of 160°C and pressure of 30 kg/cm^2. Three types of syntactic foams were fabricated with 20 wt.%, 40 wt.% and 60 wt.% cenospheres and referred to as HDPE20, HDPE40 and HDPE60, respectively. Cylindrical specimens of 7 mm diameter and 3.5 mm height were cut by an Osborne No. 149 arch punch for compression testing.

Quasi-Static Compression

Quasi-static compression testing was performed on an Instron 4467 Universal Testing System with a 30-kN load cell. Bluehill 2.0 software was used for data acquisition. Tests were conducted at 10^{-4} s^{-1}, 10^{-3} s^{-1} and 10^{-2} s^{-1} initial strain rates, corresponding to cross-head displacement velocities of 0.02 mm/min, 0.2 mm/min and 2 mm/min, respectively. The end of the test criteria was set at 70% strain. The data was analyzed using an in-house developed MATLAB code, and yield strength and modulus were calculated for every specimen.

High Strain Rate Testing

HSR compression tests were constructed using a split-Hopkinson pressure bar (SHPB) system. The length and diameter of Inconel alloy incident and

Table I. Chemical analysis details of cenospheres

Chemical analysis	
SiO_2	52–62%
Al_2O_3	32–36%
CaO	0.1–0.5%
Fe_2O_3	1–3%
TiO_2	0.8–1.3%
MgO	1–2.5%
Na_2O	0.2–0.6%
K_2O	1.2–3.2%

transmitter bars were 200 cm and 1.27 cm, respectively. Young's modulus of 200 GPa and density of 8497 kg/m^3 were taken for the Inconel alloy in calculations. Dow Corning 111 lubricant was used between the specimen and the bars. A brass pulse shaper was used at the front end of the incident bar. The incident, reflected, and transmitted strain pulses were acquired by two strain gages of type CEA-13-240UZ-120 (Vishay Precision Group, Malvern, PA, USA) that are bonded at the midpoint of the bars. The acquired pulses were recorded by a Tektronix TDS 2014B (Beaverton, OR, USA) oscilloscope. The specimen's response over time is calculated by

$$\dot{\varepsilon}(t) = \frac{2c_b\varepsilon_r(t)}{l_0} \quad (1)$$

$$\sigma(t) = \frac{AE\varepsilon_t(t)}{A_0} \quad (2)$$

$$\varepsilon(t) = \int_0^t \dot{\varepsilon}(\tau)\mathrm{d}\tau \quad (3)$$

where ε_r and ε_t are reflected and transmitted pulses, respectively, $\dot{\varepsilon}(t)$ is the strain rate obtained within the specimen, τ is the time variable used in integration, $\sigma(t)$ is the stress within the specimen, c_b is the sound wave velocity in the bar, A and E are the cross-sectional area and Young's modulus of the bar material, respectively, while l_0 and A_0 are the length and cross-sectional area of the specimen, respectively.[24]

Imaging

A Hitachi S-3400 N scanning electron microscope was used for imaging. The microscope is equipped with backscatter and secondary electron detectors. The specimens were coated with gold using a Cressington 108 auto sputter coater before imaging.

RESULTS

Syntactic Foam Microstructure

The microstructure of a representative HDPE40 specimen is shown in Fig. 1a. It can be seen that a large number of cenospheres survived the PIM process. The process was optimized in a previous study to reduce the cenosphere fracture.[23] Experimentally measured densities, along with theoretical estimates using rule of mixtures, are presented in Table II. HDPE60 syntactic foams show the highest cenosphere loading of 66.4 vol.%. Fracture of cenospheres increases with cenosphere content due to increased particle to particle interactions. Figure 1 shows that the cenospheres have defects in their walls and imperfect structures, which contribute to their lower than expected strength. These particles have a higher tendency to break compared to the engineered defect-free glass particles.[10] The low cost of the cenospheres is a driving force for their use as fillers in developing composite materials, and the results obtained on the density and mechanical properties will help in understanding the limits on the possible upper bound on the cenosphere volume fraction in the syntactic foam. In the present case, it appears that the cenosphere fracture is under 7% for syntactic foams filled with up to 40 wt.% cenospheres, which is similar to many previous studies on epoxy and vinyl ester matrix systems.[10,25] Higher particle filling results in increased fracture of cenospheres due to increased interaction between particles during pre-mixing and injection-molding steps. There is a possibility that the fractured particles become stress concentration sites, especially because of their thin-walled geometry, and adversely affect the mechanical properties of the syntactic foams. However, even with the failed particles, fabricating syntactic foam components that are non-load-bearing can provide a saving of HDPE resin.

Industrial-scale machines have been used in the previous and current studies to understand the possibility of manufacturing these materials at component-scale. It has been observed that the particle–matrix interface is not strong in these syntactic foams. Most of the current applications of syntactic foams rely on their compressive properties. It has been observed in previous studies that the tensile and flexural properties are strongly affected by the interfacial bonding strength[26–29] because the interfacial cracks tend to open up under such loading. However, the compressive properties are relatively less sensitive to interfacial bonding because the matrix is pushed on the particle during deformation.[25,30] Figure 1b shows pores in the cenosphere wall and other defects, which are expected to reduce the properties of these particles and the fabricated syntactic foams compared to the level expected with particles that have defect-free walls. The reduction in the properties due to the defects will be estimated using theoretical models.

Quasi-Static Compression

Experimental Results

The quasi-static compressive stress–strain plots for the HDPE resin and syntactic foams at different strain rates are presented in Fig. 2. The stress–strain behavior of HDPE syntactic foams is different from that observed for epoxy and vinyl ester matrix syntactic foams. Since epoxy and vinyl ester resins are brittle, a significant drop in stress is observed at the end of the initial linear elastic region followed by a stress plateau.[10,31,32] The drop of stress is due to successive failure of brittle particles in the matrix because of stress concentration in the localized region around broken particles.[33] Such effects are mitigated in significantly more compliant HDPE resin above its glass transition temperature (T_g) at

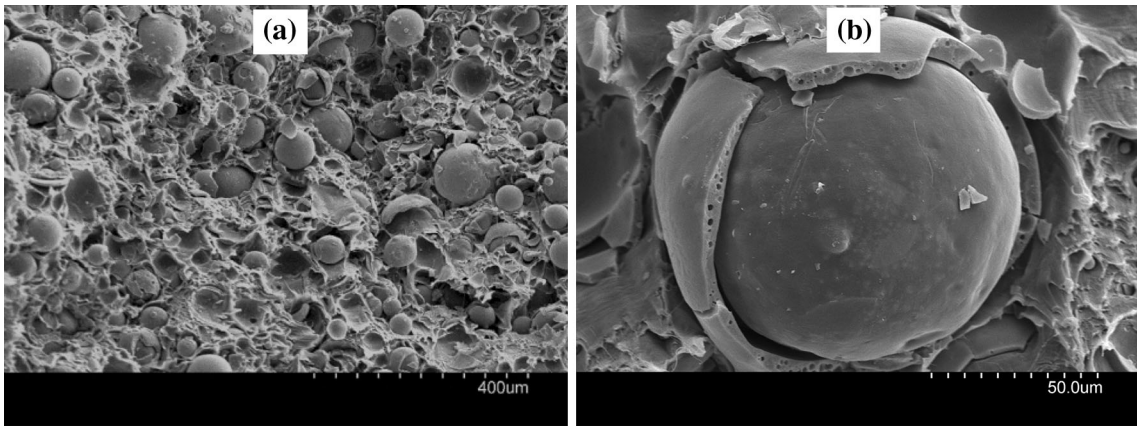

Fig. 1. Scanning electron micrographs of (a) a freeze-fractured HDPE40 specimen, (b) porosity embedded in the walls and non-uniform wall thickness can be noted in a cenosphere.

Table II. Theoretical and experimental density values of syntactic foams and cenosphere breakage during fabrication

Syntactic foam type	Φ_f	Density (g/cm^3)		Cenosphere failure during fabrication (%)
		Measured	Theoretical	
HDPE20	0.229	1.0159 ± 0.0016	0.9976	1.83
HDPE40	0.442	1.0078 ± 0.0036	0.9430	6.87
HDPE60	0.664	1.0219 ± 0.0071	0.8923	14.5

Φ_f = Cenospheres by vol.%.

room temperature. Figure 2 also indicates that the strength and modulus of HDPE and syntactic foams increase with strain rate. As shown in Fig. 3, the representative curve can be divided into three regions: (1) the initial elastic region with constant slope, (2) a post-yield plastic deformation region with smaller slope and (3) plastic deformation region with higher and increasing slope that appears after densification. There is no clearly distinguishable stress plateau region that is a characteristic of foams and porous materials; instead, the thermoplastic syntactic foams continue to harden at all strains.

The measured mechanical properties of syntactic foams are presented in Table III. Although some of the values have overlapping standard deviations, the average elastic modulus and compressive yield strength are observed to increase with strain rate for syntactic foams. HDPE40 shows the highest yield strength for all compressive strain rates among all syntactic foams. Compared to the yield strength of neat resin, the yield strengths at 10^{-2} s^{-1}, 10^{-3} s^{-1} and 10^{-4} s^{-1} strain rates for HDPE20, HDPE40 and HDPE60 are –0.3%, 9.8%, 14.2%; 7.2%, 9.3%, 17.1%; and 40.8%, 37.9%, and 31.1%, respectively, higher. The slope and y-intercept for linear trends of yield strength with respect to strain rates are presented in Table IV. Specific compressive yield strengths (ratio of yield strength and experimentally measured density) of the materials are depicted by Fig. 4 for various material compositions. Some of the syntactic foams are found to have higher performance than the neat resin. These compositions are useful in reducing the use of thermoplastic resin in relevant applications. It is also anticipated that further optimization of the process may result in reduction in crushed particles during syntactic foam fabrication, which will provide syntactic foams with lower densities and improve the weight-saving benefits.

A method devised by Smith et al.[34] is used to determine the densification point. $E_{t,0.01}(\varepsilon)$ is assumed to be the tangent modulus at strain ε of the material determined by performing a linear regression on the stress–strain curve over the range $(\varepsilon - 0.01, \varepsilon + 0.01)$, and $E_{t,0.01}(\varepsilon_y)$ to be the tangent modulus at the yield strain. The densification strain is then defined as the minimum strain for which the tangent modulus becomes greater than the value of tangent modulus at the yield point.

$$\varepsilon_d = \min\left(\varepsilon : E_{t,0.01}(\varepsilon) > E_{t,0.01}(\varepsilon_y)\right) \quad (4)$$

The densification stresses and strains obtained by this method are presented in Table III. The corresponding densification stresses are also reported.

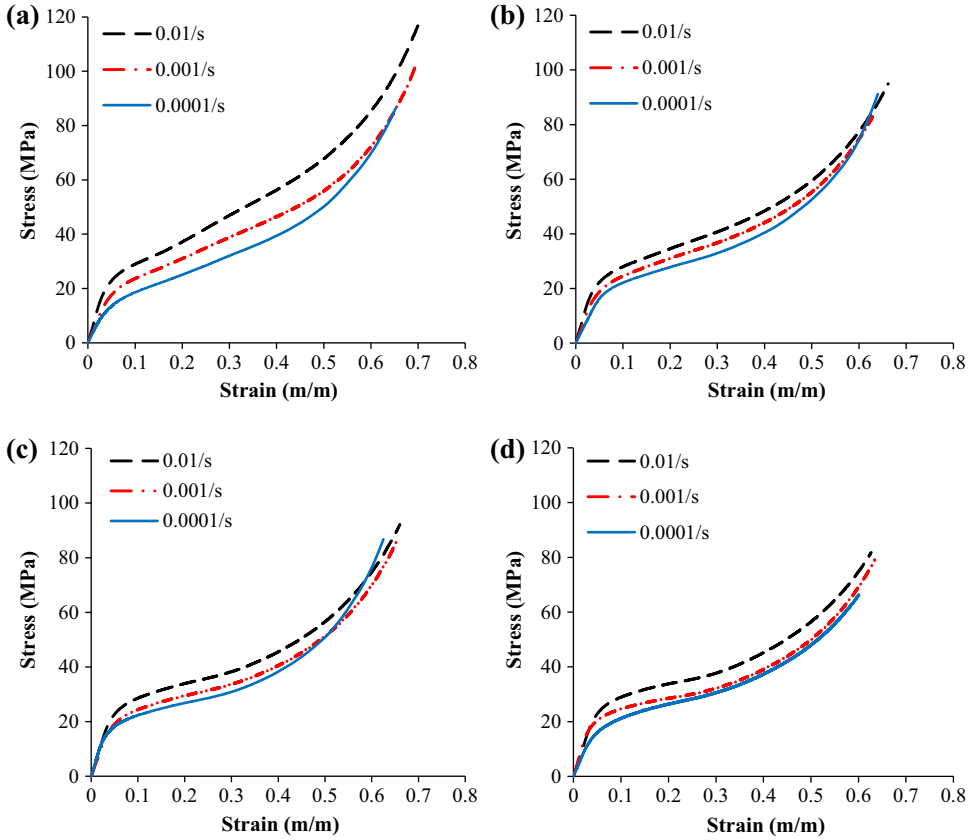

Fig. 2. Comparison of stress–strain curves at different quasi-static compressive strain rates for (a) HDPE, (b) HDPE20, (c) HDPE40 and (d) HDPE60.

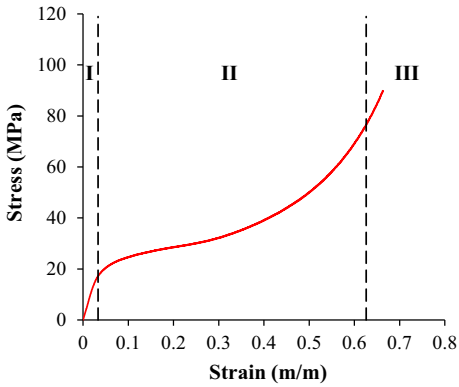

Fig. 3. A representative compressive stress–strain curve at 10^{-3} strain rate for HDPE60 syntactic foam showing three regions of different deformation behaviors (I elastic deformation, II post-yield plastic deformation, III plastic deformation beyond densification).

The densification strain decreases as strain rate is increased from 10^{-4} s^{-1} to 10^{-2} s^{-1} for all syntactic foams.

SEM images of the compressed samples are presented in Fig. 5. It can be observed that some cenospheres are intact in all the syntactic foams even after densification strain is reached. The thicker-walled cenospheres having high strength are likely to survive the compression process. Extensive deformation of the matrix and debris from fractured cenospheres are visible in all these figures. Although the compressive strain rate is changed by two orders of magnitude, the difference is not high enough to provide any change in the failure mode of syntactic foams as seen from these figures. These features will be useful in studying the HSR failure features.

Theoretical Modeling

Several theoretical models are available for estimating the elastic properties of syntactic foams.[2] These models have been developed for epoxy and vinyl ester matrix syntactic foams and found to be in good agreement with experimental data.[25] One of these models, which is based on a differential scheme pertaining to dilute dispersion of hollow particles in a matrix, has been applied to the cenosphere/HDPE syntactic foams.[25,35] The differential scheme is as follows

$$\frac{dE}{E} = f_E(E_c, \upsilon_c, E_m, \upsilon_m, \eta)\frac{d\Phi_f}{1-\Phi_f/\Phi_m} \tag{5}$$

where E_i and ν_i are the Young's modulus and Poisson's ratio, respectively, and the subscript i can be specialized as c for the ceramic particle wall material and as m for the matrix material. In

Table III. Mechanical properties for HDPE and its composites under varying low strain rate compression conditions

Material	Strain rate (s^{-1})	Elastic modulus (MPa)	Yield strength (MPa)	Yield strain (%)	Energy absorption to 50% strain (MJ/m^3)	Densification stress (MPa)	Densification strain (%)
HDPE	10^{-4}	406 ± 56	10 ± 1.0	2.8 ± 0.1	16 ± 1.1	–	–
	10^{-3}	454 ± 46	14 ± 1.4	3.1 ± 0.5	17 ± 0.7	–	–
	10^{-2}	572 ± 23	17 ± 0.5	3.2 ± 0.2	21 ± 0.2	–	–
HDPE20	10^{-4}	358 ± 16	14 ± 2.3	4.3 ± 0.8	15 ± 0.5	70 ± 2.1	58 ± 1.8
	10^{-3}	460 ± 17	15 ± 0.9	3.4 ± 0.1	17 ± 0.4	81 ± 0.7	62 ± 0.5
	10^{-2}	532 ± 58	17 ± 0.7	3.5 ± 0.4	18 ± 0.6	100 ± 7.5	66 ± 2.6
HDPE40	10^{-4}	471 ± 28	14 ± 0.8	3.8 ± 0.8	15 ± 0.6	67 ± 2.7	56 ± 2.1
	10^{-3}	472 ± 17	15 ± 0.7	3.4 ± 0.1	16 ± 0.2	77 ± 1.3	63 ± 0.5
	10^{-2}	545 ± 14	19 ± 0.4	3.7 ± 0.1	18 ± 0.2	88 ± 2.2	65 ± 0.6
HDPE60	10^{-4}	451 ± 36	14 ± 0.5	3.2 ± 0.1	17 ± 2.5	66 ± 4.2	49 ± 6.2
	10^{-3}	519 ± 45	16 ± 2.4	3.3 ± 0.6	16 ± 0.2	77 ± 7.1	63 ± 1.0
	10^{-2}	546 ± 25	20 ± 0.5	4.0 ± 0.3	18 ± 0.3	83 ± 2.9	63 ± 3.1

Table IV. Slope and *y*-intercept values of yield strength (MPa) trend lines with respect to varying low strain rates for the different composites

Material type	Slope (MPa s)	*y*-intercept (MPa)
HDPE	574	12
HDPE20	273	14
HDPE40	459	14
HDPE60	534	14

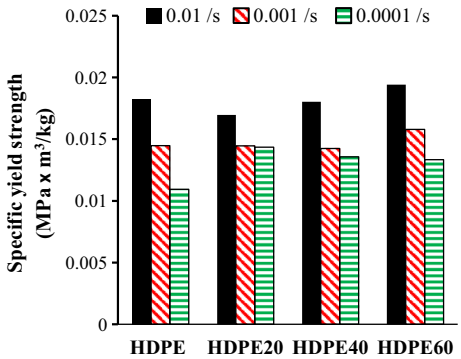

Fig. 4. Yield strength of HDPE and its syntactic foams normalized by their density at different compressive strain rates.

addition, Φ_f is the cenosphere volume fraction and Φ_m is the maximum packing factor of the particles. Since the fly ash cenospheres are not manufactured by a controlled method, the sizes of the particles may vary and the packing factor cannot be accurately calculated. Hence, it is assumed in this study that the particle size is uniform and the maximum packing factor is taken to be 0.637. Poisson's ratio for the matrix material, HDPE, is taken to be 0.425[23] and the modulus of elasticity is taken from the experiments. For the purpose of modeling, experimental results from compression tests at 10^{-3} s^{-1} strain rate are used. The ceramic wall material is a mixture of several constituent materials, as presented in Table I, and the rule of mixtures method described by[25] is used to determine the properties of ceramic walls. Ignoring minor constituents, the modulus and Poisson's ratio of cenosphere wall material are estimated to be 157 MPa and 0.19, respectively. The radius ratio of the hollow articles is represented by η and is defined as the ratio of the inner radius to the outer radius of the cenospheres. Assuming that the cenosphere walls are fully dense and uniform, the radius ratio is determined by

$$\eta = \sqrt[3]{1 - \frac{\rho_{\mathrm{TPD}}}{\rho_{\mathrm{c}}}} \tag{6}$$

where ρ_{TPD} is the true particle density and ρ_{c} is the density of the ceramic, obtained by the rule of mixtures for cenospheres considering alumino-silicate composition. Due to defects in the cenospheres walls, the effective properties of cenospheres cannot be meaningfully measured by experimentation. Thereby, parametric studies based on theoretical models are conducted to estimate cenospheres properties. As shown in Fig. 6a, experimental values of the modulus for the syntactic foams match with the parametric curve when η = 0.9975, while the ceramic wall material properties are kept constant at E_{c} = 157 GPa. Similar close agreement is seen for E_{c} = 3.75 GPa as the ceramic modulus is varied and the radius ratio obtained by density measurements is kept constant corresponding to an estimated value of η = 0.9 (Fig. 6b). The Poisson's ratio, ν_{c} = 0.19, is kept constant for both approaches. These calculations yield two sets of properties which are then used to calculate an effective modulus for the cenosphere particles by the method developed in,[36] which is given as

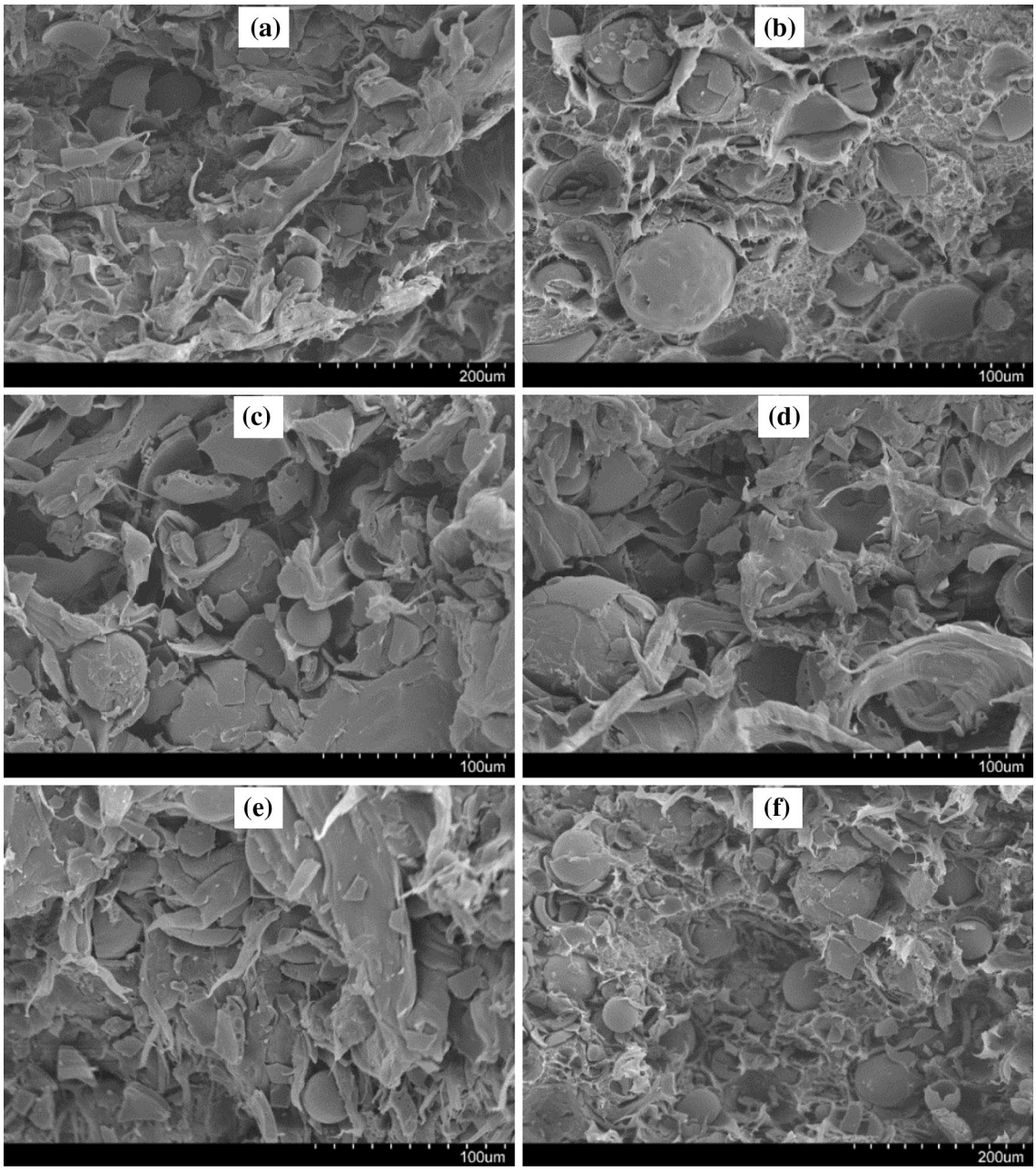

Fig. 5. SEM image of compressed (a) HDPE20 specimen at 0.01 s^{-1}, (b) HDPE20 specimen at 0.001 s^{-1}, (c) HDPE40 compressed at 0.01 s^{-1}, (d) HDPE40 specimen at 0.001 s^{-1}, (e) HDPE60 specimen at 0.001 s^{-1}, and (f) HDPE60 specimen at 0.01 s^{-1}. Intact cenospheres are found in the material even after densification strain is reached. No significant change in the failure mode is observed in the material even after two orders of magnitude change in strain rate.

$$\bar{E} = \frac{E_c(1-2\nu)(1-\eta^3)}{(1-2\nu)+\left(\frac{1+\nu}{2}\right)\eta^3} \tag{7}$$

Equation 7 yields an effective modulus of 0.60 GPa for the cenospheres from both sets of input parameters obtained earlier. A similar level of reduction in the effective properties of hollow particles was observed for SiC particles with porous walls.[37,38] Selection of higher quality particles is possible through additional processing steps such as pressurization of the particles and selecting the survivors, but such steps result in added costs, which would have to be justified by a significant increase in the material properties of syntactic foams. Since this model assumed perfect bonding between the cenospheres and the matrix, the results may vary if no bonding is assumed. Also, defects and changes in wall thickness greatly influence material properties.[39]

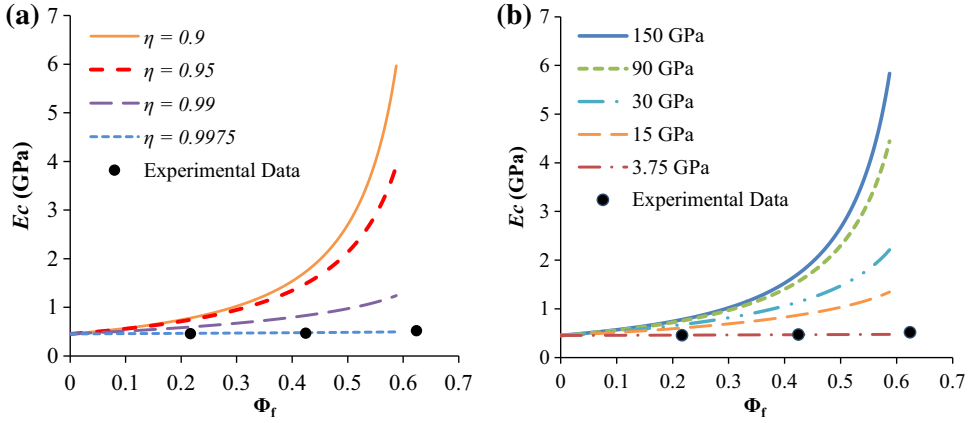

Fig. 6. Parametric study results for modulus of syntactic foams obtained from the Porfiri–Gupta model: (a) particle wall material modulus is kept constant at calculated E_c = 157 GPa and radius ratio is varied, and (b) radius ratio is kept constant at calculated η = 0.9 and the particle wall material modulus is varied.

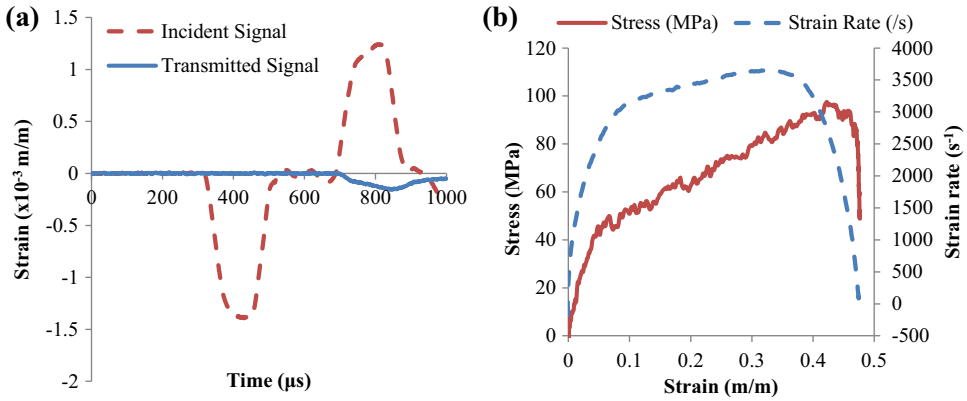

Fig. 7. A representative set of strain signals for HDPE tested at 3430 s^{-1} showing (a) incident and transmitted signals and (b) stress and strain rate with respect to strain.

High Strain Rate Compression

A representative set of strain histories obtained from the incident and transmitted bars during SHPB testing is shown in Fig. 7a for a randomly selected HDPE specimen to illustrate general trends. Equations 1–3 assume that the specimen is under dynamic stress equilibrium and is experiencing a constant strain rate during deformation.[40] The radial inertia and dispersion effects are neglected in this calculation. The strain rate reported is the average of nearly constant strain rate regions in the strain rate–strain curve shown in Fig. 7b.

The HSR stress–strain relationships at selected strain rates for HDPE and syntactic foams are presented in Fig. 8. The slope of curve in the plastic region decreases as the cenosphere content is increased. This trend is attributed to the higher strain rate sensitivity of HDPE compared to the particle material. The strain rate cannot be directly controlled during the SHPB setup and is recovered from the test results, so the graphs for various syntactic foam compositions are not compared at the exact same strain rates. Yield strength values are compared in Fig. 9 for different strain rates. It can be observed in this figure that yield strength increases with strain rate for HDPE20 and HDPE40. The results for HDPE60 show that the yield strength saturates at higher strain rates. Figure 9 shows that the yield strength values are higher than those obtained under quasi-static compression. For example, yield stress for HDPE20 syntactic foam at 3350 s^{-1} strain rate is 2.73, 3.20 and 3.23 times higher than those at 10^{-2} s^{-1}, 10^{-3} s^{-1} and 10^{-4} s^{-1} strain rates, respectively. Furthermore, for HDPE40 and HDPE60, the yield strength increases at high strain rates. The factor of increase is found to be between 1.91 and 2.54. These results show a strong strain rate sensitivity in the compressive yield strength for HDPE matrix syntactic foams.

Figure 10 presents SEM images of syntactic foam specimens compressed at strain rates around 1800 s^{-1}. Since the maximum strain that the SHPB test could provide at this strain rate was around

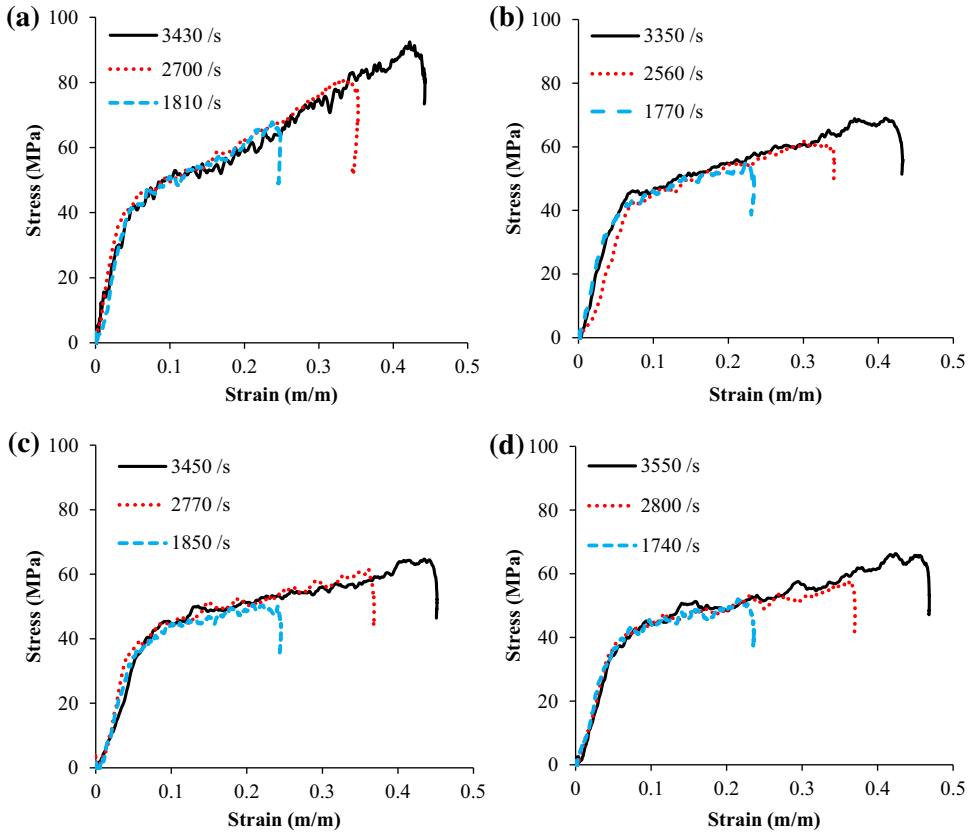

Fig. 8. Compressive stress–strain curves at three different high strain rates for (a) HDPE, (b) HDPE20, (c) HDPE40 and (d) HDPE60. The strain rates are recovered from the test results so they are not exactly the same for all materials.

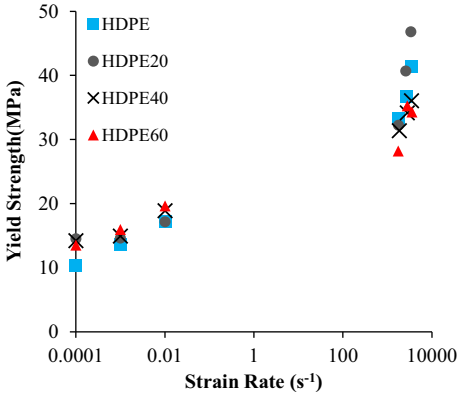

Fig. 9. Yield strength of HDPE and its syntactic foams at low and high strain rates.

0.25, several surviving cenospheres are observed from these micrographs, as densification was not completed at this strain. It should be noted that the end of the stress–strain curve in Fig. 8 does not necessarily represent specimen failure. SHPB is a wave propagation technique with a finite width of the strain pulse which is used to compress the specimen. If the specimen does not fail, the end of the test means that strain pulse reflected back in the incident bar and the specimen loading was terminated.

Increases in the specimen temperature may be a concern during rapid compression at high strain rates. Due to the short time scale during high speed compression, the heat generated in the specimen may not be dissipated. Since T_g of HDPE is below the testing temperature, changes in temperature during the test may cause significant impacts on the measured properties. The temperature of the specimens is calculated as a function of strain, assuming that κ is the fraction of the work that goes in heating of the specimen.

$$\kappa \Delta W \approx \Delta Q \tag{8}$$

$$\kappa \int_0^{\varepsilon} \sigma d\varepsilon = \rho C_v \Delta T \tag{9}$$

$$\Delta T = \frac{\kappa}{\rho C_v} \int_0^{\varepsilon} \sigma \mathrm{d}\varepsilon \tag{10}$$

where ΔW is the work done, ΔQ is the heat generated, σ is the true stress, ε is the true strain, ρ is the material density, C_v is the specific heat capacity at constant volume (plastic flow is essentially isochoric) and ΔT is the rise in temperature,

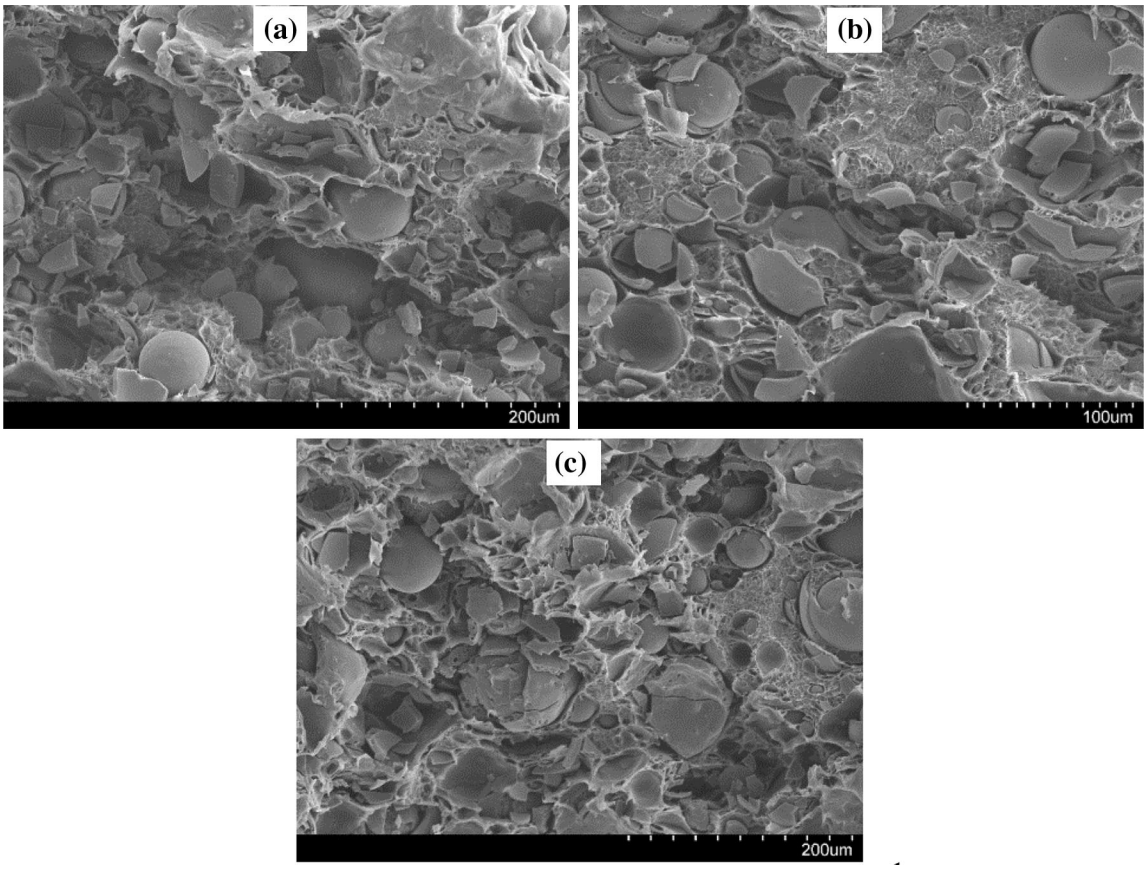

Fig. 10. SEM images of (a) HDPE20 specimen compressed at 1770 s^{-1}, (b) HDPE40 specimen compressed at 1850 s^{-1} and (c) HDPE60 specimen compressed at 1740 s^{-1}.

Table V. Storage modulus and loss modulus values of HDPE at different temperatures[42]

Temperature (°C)	Storage modulus (MPa)	Loss modulus (MPa)
25	1299	75
30.2	1207	88
34.6	1124	97
41.1	996	107

$\kappa = 1$, assuming all the work is used to heat the sample without any heat loss,[41] which will provide the upper bound in the temperature rise.

For HDPE compressed at 25°C under 3430 s^{-1}, 2700 s^{-1} and 1810 s^{-1} strain rates, the calculated temperature rise is 16.1°C, 9.6°C and 5.2°C, respectively. A functional relationship between Young's modulus and temperature is not available for HDPE. However, viscoelastic properties of HDPE have been documented by Sewda et al.[42] and Kim et al.[33] with respect to temperature. These studies provide a relationship between temperature and the storage and loss moduli of HDPE resin. The storage and loss moduli of HDPE at 20°C are 1299 MPa and 75 MPa, respectively,[42] but the storage modulus reduces to 996 MPa and loss modulus increases to 107 MPa at 41.1°C, as listed in Table V. These results show that an increase in temperature may have an effect in the measured high strain rate properties.

CONCLUSIONS

Plastic injection molding was used to synthesize HDPE syntactic foams containing 20 wt.%, 40 wt.% and 60 wt.% fly ash cenospheres. Samples of these syntactic foams were then studied for compressive properties at quasi-static and high strain rates. A theoretical model was used to estimate the properties of cenospheres based on the experimental results on syntactic foams. Temperature rise during HSR compression was calculated using an analytical expression. The results of the study can be summarized as:

- Several compositions of syntactic foams can have higher yield strength than the matrix material. Syntactic foam compositions can also be identified to have higher specific yield strength than the neat matrix material. This observation points to possibilities of weight saving by using syntactic foams.

- The yield strengths under HSR were found to be greater than those under quasi-static or low strain compression, with higher strain rate sensitivity as the percentage of cenospheres was increased.
- Modulus of elasticity for HDPE and syntactic foams increases with strain rates in the quasi-static strain rate regime.
- In the present investigation, it is apparent that the 60 wt.% of cenospheres is too high to have high-quality syntactic foams because of cenosphere fracture due to particle to particle interaction during mixing. Syntactic foams with 40 wt.% cenospheres have better quality and properties.

ACKNOWLEDGEMENTS

Authors acknowledge Dr. Keshav Prabhu, Mr. Puneeth and Mr. Praveen of Konkan Speciality Polyproducts Pvt. Ltd., Mangalore, Karnataka, India for providing the Injection molding facility for casting the samples and useful discussions. Author Gupta acknowledges the Office of Naval Research Grant N00014-10-1-0988. The views expressed in this article are those of authors, not of funding agencies. The authors thank the ME Department at NIT-K and MAE Department at NYU for providing facilities and support. Steven E. Zeltmann is thanked for help with manuscript preparation and technical discussions.

REFERENCES

1. P.K. Rohatgi, D. Weiss, and N. Gupta, *JOM* 58, 71 (2006).
2. D. Luong, N. Gupta, A. Daoud, and P. Rohatgi, *JOM* 63, 53 (2011).
3. F. Shutov, *Syntactic polymer foams. Chromatography/Foams/Copolymers*, vol. 73/74 Advances in Polymer Science, (Berlin: Springer, 1986), p. 63.
4. N. Gupta, Kishore, E. Woldesenbet, and S. Sankaran, *J. Mater. Sci.* 36, 4485 (2001).
5. F. Grosjean, N. Bouchonneau, D. Choqueuse, and V. Sauvant-Moynot, *J. Mater. Sci.* 44, 1462 (2009).
6. X. Lefebvre, V. Sauvant-Moynot, D. Choqueuse, and P. Chauchot, *Oil Gas Sci. Technol.—Revue d'IFP Energies nouvelles* 64, 165 (2009).
7. N. Gupta and E. Woldesenbet, *Compos. Struct.* 61, 311 (2003).
8. B. John, C.P.R. Nair, K.A. Devi, and K.N. Ninan, *J. Mater. Sci.* 42, 5398 (2007).
9. G. Gladysz, B. Perry, G. McEachen, and J. Lula, *J. Mater. Sci.* 41, 4085 (2006).
10. N. Gupta, R. Ye, and M. Porfiri, *Compos. B* 41, 236 (2010).
11. N. Gupta, S. Zeltmann, V. Shunmugasamy, and D. Pinisetty, *JOM* 66, 245 (2013).
12. N. Gupta, D. Pinisetty, and V.C. Shunmugasamy, *Reinforced Polymer Matrix Syntactic Foams: Effect of Nano and Micro-Scale Reinforcement* (Hoboken: Springer International Publishing, 2013).
13. B. Song, W. Chen, and D.J. Frew, *J. Compos. Mater.* 38, 915 (2004).
14. B. Song, W. Chen, T. Yanagita, and D.J. Frew, *Compos. Struct.* 67, 279 (2005).
15. R.L. Poveda and N. Gupta, *Int. J. Crashworthiness* 17, 497 (2012).
16. D.F. Sounik, P. Gansen, J.L. Clemons, and J.W. Liddle, *SAE Trans.* 106, 211 (1997).
17. P. Li, N. Petrinic, C.R. Siviour, R. Froud, and J.M. Reed, *Mater. Sci. Eng. A* 515, 19 (2009).
18. W.A. Waite, M.L. Waldron, and A. Nahabedian, *Nav. Eng. J.* 81, 95 (1969).
19. B. Song, W. Chen, T. Yanagita, and D.J. Frew, *Compos. Struct.* 67, 289 (2005).
20. M.C. Boyce, D.M. Parks, and A.S. Argon, *Mech. Mater.* 7, 35 (1988).
21. N. Gupta and W. Ricci, *Mater. Sci. Eng. A* 427, 331 (2006).
22. N. Gupta and E. Woldesenbet, *J. Cell. Plast.* 40, 461 (2004).
23. B.R. Bharath Kumar, M. Doddamani, S.E. Zeltmann, N. Gupta, M.R. Ramesh, and S. Ramakrishna, *Mater. Des.* 2016, 414 (2016).
24. J. Shim and D. Mohr, *Int. J. Impact Eng.* 36, 1116 (2009).
25. M. Aureli, M. Porfiri, and N. Gupta, *Mech. Mater.* 42, 726 (2010).
26. B.R. Bharath Kumar, M. Doddamani, S.E. Zeltmann, N. Gupta, Uzma, S. Gurupadu, and R.R.N. Sailaja, *J. Mater. Sci.* 51, 3793 (2016).
27. B.R. Bharath Kumar, S.E. Zeltmann, M. Doddamani, N. Gupta, Uzma, S. Gurupadu, and R. R. N. Sailaja, National Institute of Technology - Karnataka, Surathkal, India, unpublished research, 2016.
28. L. Zhang and J. Ma, *Compos. Sci. Technol.* 70, 1265 (2010).
29. L. Yusriah and M. Mariatti, *J. Compos. Mater.* 47, 169 (2013).
30. G. Tagliavia, M. Porfiri, and N. Gupta, *Int. J. Solids Struct.* 47, 2164 (2010).
31. E.M. Wouterson, F.Y.C. Boey, X. Hu, and S.-C. Wong, *Compos. Sci. Technol.* 65, 1840 (2005).
32. L. Zhang, S. Roy, Y. Chen, E.K. Chua, K.Y. See, X. Hu, and M. Liu, *ACS Appl. Mater. Interfaces* 6, 18644 (2014).
33. J.I. Kim, S.H. Ryu, and Y.W. Chang, *J. Appl. Polym. Sci.* 77, 2595 (2000).
34. B.H. Smith, S. Szyniszewski, J.F. Hajjar, B.W. Schafer, and S.A. Arwade, *Metals* 2, 399 (2012).
35. M. Porfiri and N. Gupta, *Compos. B* 40, 166 (2009).
36. G. Li, Y. Zhao, and S.-S. Pang, *Mater. Sci. Eng. A* 271, 43 (1999).
37. M. Labella, V.C. Shunmugasamy, O.M. Strbik, and N. Gupta, *J. Appl. Polym. Sci.* 131, 40689 (2014).
38. V.C. Shunmugasamy, S.E. Zeltmann, N. Gupta, and O.M. Strbik III, *JOM* 66, 892 (2014).
39. K.B. Carlisle, M. Lewis, K.K. Chawla, M. Koopman, and G.M. Gladysz, *Acta Mater.* 55, 2301 (2007).
40. M.D. Goel, V.A. Matsagar, A.K. Gupta, and S. Marburg, *Trans. Nonferr. Met. Soc. China* 23, 1080 (2013).
41. R. Kapoor and S. Nemat-Nasser, *Mech. Mater.* 27, 1 (1998).
42. K. Sewda and S.N. Maiti, *Polym. Bull.* 70, 2657 (2013).